Bipedal Robust Walking on Uneven Footholds: Piecewise Slope LIPM with Discrete Model Predictive Control

Yapeng Shi[1*], Sishu Li[1,2*], Yongqiang Wu[1], Junjie Liu[1], Xiaokun Leng[1], Xizhe Zang[2] and Songhao Piao[1]

Abstract—This study presents an enhanced theoretical formulation for bipedal hierarchical control frameworks under uneven terrain conditions. Specifically, owing to the inherent limitations of the Linear Inverted Pendulum Model (LIPM) in handling terrain elevation variations, we develop a Piecewise Slope LIPM (PS-LIPM). This innovative model enables dynamic adjustment of the Center of Mass (CoM) height to align with topographical undulations during single-step cycles. Another contribution is proposed a generalized Angular Momentum-based LIPM (G-ALIP) for CoM velocity compensation using Centroidal Angular Momentum (CAM) regulation. Building upon these advancements, we derive the DCM step-to-step dynamics for Model Predictive Control MPC formulation, enabling simultaneous optimization of step position and step duration. A hierarchical control framework integrating MPC with a Whole-Body Controller (WBC) is implemented for bipedal locomotion across uneven stepping stones. The results validate the efficacy of the proposed hierarchical control framework and the theoretical formulation.

I. INTRODUCTION

Achieving adaptive bipedal locomotion across uneven terrains, particularly those with restricted footholds such as uneven stepping stones (Fig. 1), remains a significant challenge in robotics. In such scenarios, the generation of walking gait patterns necessitates the synthesis among optimal step position, step duration, and Ground Reaction Forces (GRFs) to ensure stability [1].

The Linear Inverted Pendulum Model (LIPM) has been extensively adopted as a computationally efficient paradigm for bipedal locomotion due to its simplified dynamics. By assuming a constant height for the Center of Mass (CoM), LIPM enables real-time motion control through linearized equations of motion [2]. This formulation has been further extended to accommodate inclined surfaces by aligning the CoM height relative to terrain slopes [3]. However, a significant limitation persists: the model inherently excludes

[1]Yapeng Shi, Sishu Li, Yongqiang Wu, Junjie Liu, Xiaokun Leng, and Songhao Piao are with the Faculty of Computing, Harbin Institute of Technology, Harbin, 150001, China `shi.yapeng@hit.edu.cn`, {`23s108219, 24s103252, 2021112637`}`@stu.hit.edu.cn`, {`lengxiaokun, piaosh`}`@hit.edu.cn`

[2]Sishu Li and Xizhe Zang are with the State Key Laboratory of Robotics and System, Harbin Institute of Technology, Harbin, 150001, China `zangxizhe@hit.edu.cn`
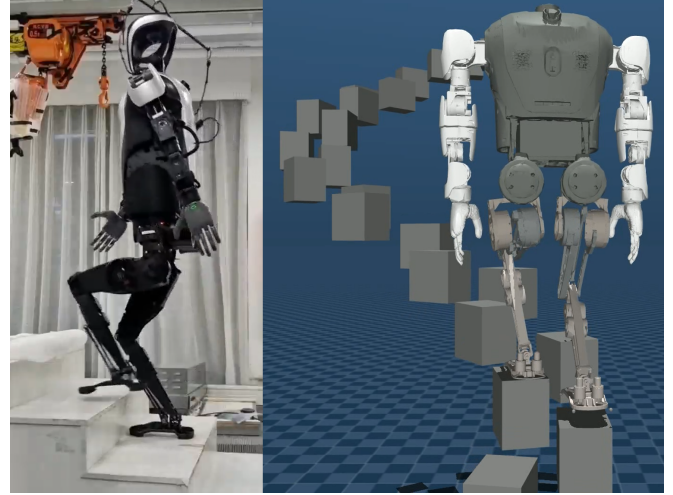
Fig. 1. Humanoid robot KUAVO with its MuJoCo simulation walking on uneven stepping stones.

consideration of variable CoM height. With predefined step position and duration, the Center of Pressure (CoP) can be modified by carefully adjusting the joint torques, thereby modulating GRFs at the contact feet. However, exclusive reliance on CoP modification imposes critical limitations. This strategy not only requires specific physical leg designs but also limits flexibility in maintaining stability under unexpected terrain changes or external disturbances [1].

Recent advancements highlight the superiority of adaptive step parameter modulation (step position and step duration) for stabilizing bipedal locomotion [4], [5]. The Divergent Component of Motion (DCM), which characterizes the unstable dynamics inherent in LIPM, provides a theoretical foundation for capturing and controlling the robot's dynamics stability during locomotion [6]. DCM-based methodologies enable robots to dynamically adjust step positions, driving CoM trajectories toward stable manifolds, even under external disturbances or foothold constraints [7], [8].

In recent years, the simultaneous adjustment of step position and step duration has been proposed using analytical [9] or optimization-based approaches [10]. Model Predictive Control (MPC) frameworks have demonstrated particular promise by optimizing step parameters within a prediction horizon, accounting for system dynamics and foothold feasibility constraints [11], [12]. This enables the robot to generate reactive walking gait patterns that ensure stability over multiple steps. Complementing MPC, the Whole-Body Controller (WBC), on the other hand, operates at a lower

level, enforces stability, handling contact dynamics, and ensuring the robot remains balanced and responsive to real-world conditions [13], [14].

Dividing vertical and horizontal dynamics, LIPM has been used for horizontal motion planning in uneven terrain loco-motion [15]. Gibson *et al.* proposes an Angular Momentum Linear Inverted Pendulum (ALIP) based controller that can walk on surfaces with varied inclinations [16]. Oluwami *et al.* introduces a variation of the ALIP model for walking stairs planning [17], demonstrates walking on periodic uneven discrete footholds. Walking on stochastic footholds in the sagittal plane has also been proposed [15]. However, they neglect critical interactions between vertical centroid motion and horizontal dynamics when there are rapid changes in terrains with varying elevations. Building upon these foundations and limitations, this study proposes a novel extended LIPM considering coupled three-dimensional dynamics, aims to advance the state-of-the-art in bipedal locomotion on uneven terrains with discrete foothold constraints.

Our principal contribution comprises two novel dynamics models: 1) the Piecewise Slope LIPM (PS-LIPM), which enables variation in the CoM height during single-step cycles, and 2) the Generalized Angular-Momentum Linear Inverted Pendulum (G-ALIP) model, which facilitates CoM velocity regulation through adjustments of the Centroidal Angular Momentum (CAM). The integration of these models establishes a DCM step-to-step dynamics, which explicitly characterizes hybrid dynamics during step transitions. As an additional contribution, we introduce an MPC-based optimization approach capable of simultaneously optimizing step position and step duration, allowing the bipedal to effectively traverse uneven terrains. To bridge the gap between reduced-order models and physical robots, we implement a hierarchical control framework that leverages a 1kHz WBC for real-time discrepancy compensation. This enhances robustness against terrain uncertainties and force disturbances. Experimental validation across a variety of challenging terrains and disturbance scenarios has confirmed the effectiveness of the framework. Comparative studies further demonstrate the superiority of PS-LIPM and G-ALIP formulations.

II. MODEL FORMULATION

A. PS-LIPM Hybrid Dynamics

LIPM simplifies the complexity of bipedal dynamics into linear equations for real-time execution. This work extends the conventional LIPM to address height-varied terrains by piecewise-slope modeling of adjacent contact surfaces with different gradients (Fig. 2). For the $x-z$ plane dynamics, the LIPM for slope surfaces is formulated as:

$$\ddot{x} = \frac{g}{\tilde{z}}x =: \omega^2 x$$
$$\tilde{z} = z - k_x x, \tag{1}$$

where x, $\dot{x}$, and $\ddot{x}$ are the position, velocity, and acceleration of the CoM, respectively, g is the gravitational acceleration, z indicates CoM height, $\tilde{z}$ specifies the vertical distance between CoM and slope surface, k_x defines the slope gradient
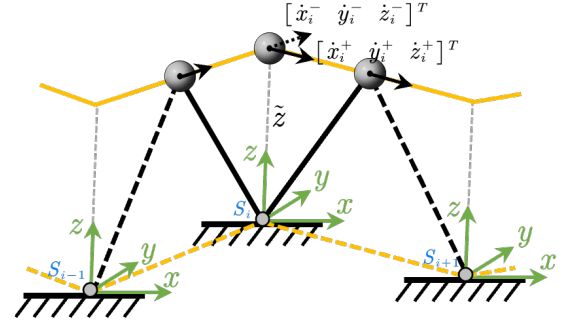

Fig. 2. As the contact point lands on the new virtual support plane (yellow dashed line), the CoM transitions from the old slope to the new slope (yellow solid line), with the velocity undergoing a sudden change at their intersection, noting that the two transitions do not occur simultaneously.

coefficient, subscript notation $(\cdot)_x$ for x direction, $(\cdot)_y$ for y direction, and $\omega = \sqrt{g/\tilde{z}}$ denotes the system's natural frequency. Without loss of generality, the current contact point $S = [S_x, S_y, S_z]^T$ is analytically set at $(0,0,0)$ to establish a local coordinate system.

The gradients of the piecewise slopes vary during the traversal of the stepping stones with random elevations. The robot must dynamically transition between piecewise slopes with distinct gradients. The following derivation is based on the assumption that velocity variations during slope transitions occur within an infinitesimal time interval, allowing them to be modeled as instantaneous state switching.

This study introduces the superscript notation $(\cdot)^-$ for pre-transition states and $(\cdot)^+$ for post-transition states to characterize dynamic switching between inclined surfaces. The CoM states defined correspondingly as: 1) Pre-transition: $[x, y, z, \dot{x}^-, \dot{y}^-, \dot{z}^-]^T$, 2) Post-transition: $[x, y, z, \dot{x}^+, \dot{y}^+, \dot{z}^+]^T$. Slope characteristics are parameterized by gradient coefficients with (k_x^-, k_y^-) and (k_x^+, k_y^+), respectively. Thus, the states must satisfy:

$$\dot{z}^- = k_x^- \dot{x}^- + k_y^- \dot{y}^-$$
$$\dot{z}^+ = k_x^+ \dot{x}^+ + k_y^+ \dot{y}^+. \tag{2}$$

Angular momentum conservation about the contact point yields:

$$L_x : m\left(y\dot{z}^- + z\dot{y}^-\right) = m\left(y\dot{z}^+ + z\dot{y}^+\right)$$
$$L_y : m\left(z\dot{x}^- - x\dot{z}^-\right) = m\left(z\dot{x}^+ - x\dot{z}^+\right), \tag{3}$$

where L_x, L_y denotes the components of angular momentum with respect to the contact point, m denotes mass of the system.

By solving Eq. (3), the following PS-LIPM dynamics can be derived:

$$\dot{x}^+ = \frac{x}{z}\Delta\dot{z} + \dot{x}^-$$
$$\dot{y}^+ = \frac{y}{z}\Delta\dot{z} + \dot{y}^- \tag{4}$$
$$\dot{z}^+ = \dot{z}^- + \Delta\dot{z}.$$

According to Eq.(2), $\Delta\dot{z}$ satisfies:

$$\Delta\dot{z} = \frac{\left(k_x^+ - k_x^-\right)\dot{x}^- + \left(k_y^+ - k_y^-\right)\dot{y}^-}{1 - k_x^+ \frac{x}{z} - k_y^+ \frac{y}{z}}. \tag{5}$$

Let $\boldsymbol{x}$ denote the robot's state vector, formally defined as:

$$\boldsymbol{x} = [x, y, \dot{x}, \dot{y}]^T \in \mathbb{R}^4, \tag{6}$$

and Δ_{com} is the corresponding reset map. Eq. (4) can be rewritten to:

$$\begin{aligned} \boldsymbol{x}^+ &= \Delta_{\text{com}}(\boldsymbol{x}^-) \\ \dot{z}^+ &= \dot{z}^- + \Delta\dot{z}. \end{aligned} \tag{7}$$

To formally distinguish between boundary states at slope transitions and general system states, we define the following hybrid system domain:

$$\begin{aligned} \mathcal{D} &= \left\{ \boldsymbol{x} \in \mathbb{R}^4 : z \neq k_x^+ x + k_y^+ y + \tilde{z} \right\} \\ \mathcal{S} &= \left\{ \boldsymbol{x} \in \mathbb{R}^4 : z = k_x^+ x + k_y^+ y + \tilde{z} \right\}. \end{aligned} \tag{8}$$

The complete hybrid dynamics of the PS-LIPM are then derived by combining Eq. (1) and Eq. (7):

$$\begin{cases} \begin{cases} \ddot{x} = \omega^2 x \\ \ddot{y} = \omega^2 y \end{cases} & \boldsymbol{x} \in \mathcal{D}/\mathcal{S} \\ \boldsymbol{x}^+ = \Delta_{\text{com}}(\boldsymbol{x}^-) & \boldsymbol{x}^- \in \mathcal{S}. \end{cases} \tag{9}$$

where Δ_{com} denotes the reset map introduced in Eq. (4).

B. G-ALIP Model

The Angular-Momentum Linear Inverted Pendulum (ALIP) model extends the classic LIPM. ALIP model explicitly includes angular momentum about the contact point as a state variable. This critical enhancement enables more physically accurate representations of bipedal dynamics:

$$\begin{bmatrix} \dot{x} \\ \dot{L}_y \end{bmatrix} = \begin{bmatrix} 0 & 1/(mz) \\ mg & 0 \end{bmatrix} \begin{bmatrix} x \\ L_y \end{bmatrix}. \tag{10}$$

Given the definition $\tilde{x}^{\text{ALIP}} = L_y/(mz)$, the Eq. 10 can be reformulated as:

$$\begin{bmatrix} \dot{x} \\ \tilde{x}^{\text{ALIP}} \end{bmatrix} = \begin{bmatrix} 0 & 1 \\ \omega^2 & 0 \end{bmatrix} \begin{bmatrix} x \\ \tilde{x}^{\text{ALIP}} \end{bmatrix}. \tag{11}$$

L_y comprises both the angular momentum of the CoM about the contact point and the CAM $L_{y,\text{com}}$:

$$L_y = mz\dot{x} - mx\dot{z} + L_{y,\text{com}}. \tag{12}$$

For a robot walking on a planar surface, $\dot{z}$ can be assumed to be zero. Thus, the velocity term $\tilde{x}^{\text{ALIP}}$ satisfies:

$$\tilde{x}^{\text{ALIP}} = \dot{x} + L_{y,\text{com}}/(mz). \tag{13}$$

This formular introduces a compensatory mechanism that converts the angular momentum to an equivalent CoM velocity when abstracting the robotic system to an inverted pendulum model. The equivalence implies instantaneous transformation of centroidal momentum from angular to linear form. In contrast, the conventional LIPM entirely neglects changes in CAM. However, the behavior of a physically realizable robot under appropriate postural control is expected to lie between these two models, with its posture gradually stabilizing over time and its CAM asymptotically approaching zero.

Therefore, we propose a G-ALIP model:

$$\tilde{x} = \dot{x} + \alpha L_{y,\text{com}}/(mz), \quad \alpha \in [0, 1]. \tag{14}$$

This model introduces a G-ALIP coefficient α to represent the conversion ratio between the CAM and linear velocity. $\alpha = 0$ corresponds to the conventional LIPM, while $\alpha = 1$ corresponds to that of ALIP model. In our work, by selecting an appropriate value for this coefficient between zero and one, the accuracy of the prediction can be improved.

III. DCM STEP-TO-STEP DYNAMICS

This section derive the step-to-step dynamics of initial DCM under extended LIPM. We first derive the hybrid dynamics of the piecewise-slope DCM under the G-ALIP framework. Then we present the preliminaries of the LIPM nominal trajectory. The asymptotical convergence of the LIP trajectory under nominal DCM is proved. Finally, the step-to-step dynamics of the DCM based on the LIP nominal trajectory approximation is ultimately presented.

Regulating the DCM ensures dynamic balance maintenance throughout the robotic walking cycle. The DCM is defined as follows:

$$\begin{cases} \xi_x = x + \frac{\tilde{x}}{\omega} \\ \xi_y = y + \frac{\dot{y}}{\omega} \end{cases}. \tag{15}$$

By combining Eq. (1) and Eq. (15), we can obtain:

$$\begin{cases} \dot{\xi}_x = \omega(\xi_x - S_x) \\ \dot{\tilde{x}} = \omega(\xi_x - x) \end{cases}. \tag{16}$$

The time evolution of the DCM is given by:

$$\xi_x(t) = (\xi_{x,0} - S_x)e^{\omega t} + S_x, \tag{17}$$

where $\xi_{x,0}$ is the initial DCM at $t = 0$. From the above formula, it can be observed that x asymptotically converges toward ξ_x, while ξ_x itself demonstrates inherent exponential divergence characteristics. This divergence property necessitates careful stability management in bipedal locomotion. As $t \to \infty$, the DCM exponentially diverges ($e^{\omega t}$ term).

The hybrid dynamics formulation of the PS-LIPM reveals critical discontinuities in the CoM velocity during slope transitions. The intrinsic coupling between ξ_x and the CoM velocity leads to discontinuous state transitions for the DCM. The DCM hybrid dynamics can be expressed as follows:

$$\begin{cases} \dot{\xi}_x = \omega(\xi_x - S_x) & \boldsymbol{x} \in \mathcal{D}/\mathcal{S} \\ \xi_x^+ = \xi_x^- + \frac{1}{\omega}(\tilde{x}^+ - \tilde{x}^-) & \boldsymbol{x}^- \in \mathcal{S} \end{cases}, \tag{18}$$

such that $[x^-, y^-, \tilde{x}^-, \tilde{y}^-]^T = \Delta_{\text{com}}([x^+, y^+, \tilde{x}^+, \tilde{y}^+]^T)$.

By solving Eq. (1), the analytical solution of the CoM state can be derived as follows:

$$x(t) = x_0 \cosh(\omega t) + \dot{x}_0 \sinh(\omega t)/\omega. \tag{19}$$

Consider a periodic motion trajectory, as depicted in Fig. 3. Let P_x denote the step length in the forward direction, W the lateral distance between the two feet, and T the step duration. The subscript $(\cdot)_i$ indicates the step index, and the subscript $(\cdot)_m$ denotes the midpoint of each motion cycle. Defining the midpoint at $t_m = 0$, the motion cycle spans the temporal domain $[-T/2, T/2]$.
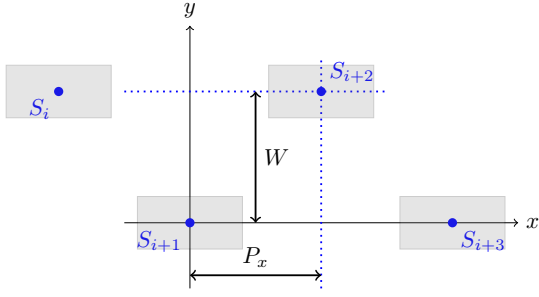
Fig. 3. Step positions of the robot during periodic motion without lateral offset. The blue dots are the step positions and the gray rectangles represent the stepping stones.

Due to symmetry, it is evident that $x_m = 0$, $\dot{y}_m = 0$ and the following relationship holds:

$$\dot{x}_m = \frac{\omega P_x}{2\sinh(\omega T/2)} \\ y_m = \frac{W}{2\cosh(\omega T/2)}. \quad (20)$$

Therefore, the periodic trajectory can be mathematically formulated as:

$$\begin{cases} x(t) = \dot{x}_m \sinh(\omega t)/\omega \\ y(t) = y_m \cosh(\omega t) + \dot{y}_m \sinh(\omega t)/\omega \end{cases}. \quad (21)$$

When introducing a lateral offset P_y in the y-direction, $\dot{x}_m$, x_m and y_m remain invariant, whereas $\dot{y}_m$ is adjusted to $\omega P_y/(2\sinh(\omega T/2))$.

Under the assumption of periodic variations in both step duration and step position, the DCM exhibits periodic behavior, yielding the nominal DCM trajectory:

$$\boldsymbol{\xi}_{0,\text{nom}} = \boldsymbol{\xi}_{0,\text{nom}} - S_{\text{init}} = \begin{bmatrix} \frac{P_x}{e^{\omega T}-1} \\ \frac{W_{l/r}}{e^{\omega T}+1} + \frac{P_y}{e^{\omega T}-1} \end{bmatrix}, \quad (22)$$

where $S_{\text{init}} = (0,0)^T$ is the initial contact point, $W_{l/r} = -W$ when the supporting leg is the left leg, and $W_{l/r} = W$ otherwise, as shown in [11].

The asymptotic convergence of the DCM to its nominal trajectory guarantees the exponential stabilization of the centroid motion to periodic orbits. Let x_{dev} represent the initial CoM position deviation at $t = -T/2$. Through substitution of this perturbed initial condition into the governing dynamics, the relationship between the initial and final states of the cycle and the nominal DCM can be expressed as follows:

$$\begin{cases} x_{-T/2} = -\frac{P_x}{2} + x_{\text{dev}} \\ x_{-T/2} + \dot{x}_{-T/2} = \frac{P_x}{e^{\omega T}-1} \\ x_{T/2} = x_{-T/2}\cosh(\omega T) + \dot{x}_{-T/2}\sinh(\omega T)/\omega \end{cases}. \quad (23)$$

The CoM position at $x_{T/2}$ can be derived as follows:

$$x_{T/2} = \frac{P_x}{2} + e^{-\omega T} x_{\text{dev}}. \quad (24)$$

As demonstrated in the derivation, the introduced initial CoM position deviation asymptotically diminishes to zero. This convergence behavior guarantees that the centroid motion ultimately stabilizes to the periodic trajectory.

The hybrid dynamics of the DCM govern the evolution of the robot's state during step durations through the coupled relationship between the DCM and centroid velocity. Given the convergence of centroid trajectories toward nominal periodic gait patterns, the actual centroid motion can be effectively approximated by its nominal trajectory. Furthermore, empirical observations reveal that slope transition timing typically coincides with the midpoint of the step cycle under normal operating conditions. These simplifications yield the following step-to-step DCM dynamics:

$$\xi_{x,T/2} = \left(\xi_{x,-T/2} - S_x\right) e^{\omega T} + \frac{\dot{x}_m^+ - \dot{x}_m^-}{\omega} e^{\omega T/2} + S_x, \quad (25)$$

such that $\boldsymbol{x}_m^+ = \Delta_{\text{com}}\left(\boldsymbol{x}_m^-\right)$.

IV. HIERARCHICAL CONTROL FRAMEWORK BASED ON DCM STEP-TO-STEP DYNAMICS

This study presents a hierarchical control framework, consisting of an MPC-based planner and a WBC, for bipedal locomotion on uneven terrains. The proposed framework abstracts discontinuous stepping-stone terrains as sequences of virtual slopes, with geometric parameters adaptively synthesized from spatial stone distributions. As shown in Fig. 4, considering the lateral foot distance W, we introduce an adjusted foothold $\tilde{S}_i^{\text{des}} = S_i^{\text{des}} + [0, W_{l/r,i}/2, 0]^T$. The adjustment enables proper virtual slope generation without direct connection of adjacent footholds. The virtual slope vector between consecutive adjusted footholds is as follows:

$$[P_{x,i}, P_{y,i}, P_{z,i}]^T = \tilde{S}_{i+1}^{\text{des}} - \tilde{S}_i^{\text{des}}. \quad (26)$$

The slope gradient is computed under the geometric constraint that the connection line between adjacent footholds remains perpendicular to the intersection line of the virtual slope plane with the xy-plane.

The slope gradient can be calculated as follows:

$$k_{x,i}^+ = k_{x,i+1}^- = \frac{P_{x,i}P_{z,i}}{P_{x,i}^2 + P_{z,i}^2} \\ k_{y,i}^+ = k_{y,i+1}^- = \frac{P_{y,i}P_{z,i}}{P_{y,i}^2 + P_{z,i}^2}. \quad (27)$$

The high-level gait planner incorporates the methodology mentioned in [11] for trajectory optimization. To formulate the trajectory optimization problem, we define the key variables:

- $\tau_i = e^{\omega T_i}$, represents the temporal variable.
- $\mathbf{b}_i = [\xi_{x,i} - S_{x,i}, \xi_{y,i} - S_{y,i}]^T$, corresponds to the DCM offset.
- $\mathbf{u}_i = [S_{x,i} - S_{x,0}, S_{y,i} - S_{y,0}]^T$, redefined as the displacement vector from the i-th step position to its current contact point S_0, rather than the previous step position. In particular, $\mathbf{u}_0 = [0,0]^T$.
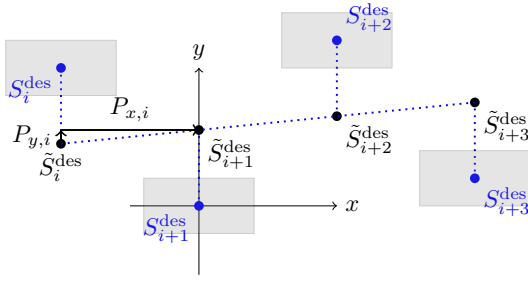
Fig. 4. Segmented slope virtual constraint generation. The blue dots are the desired step positions and black dots are adjusted step positions used to generate virtual slope considering the fixed step width W.

With the aforementioned definitions of symbols, by substituting $\xi_{x,i-1}$ and $\xi_{x,i}$ into Eq. (25), we can derive the solution as follows:

$$\tau_i \mathbf{b}_{i-1} - \mathbf{b}_i = \mathbf{u}_i - \mathbf{u}_{i-1} + \begin{bmatrix} \frac{\dot{x}_{m,i}^+ - \dot{x}_{m,i}^-}{\omega} \\ \frac{\dot{y}_{m,i}^+ - \dot{y}_{m,i}^-}{\omega} \end{bmatrix} e^{\omega T_i/2}. \tag{28}$$

We aim to make the aforementioned parameters as close as possible to the desired values:

- $\tau_{i,\text{nom}} = e^{\omega T_{i,\text{nom}}}$, $T_{i,\text{nom}} = 0.5\,\text{s}$.
- $\mathbf{b}_{i,\text{nom}} = \boldsymbol{\xi}_{0,\text{nom}}$, this desired value is for maintaining balance.
- $\mathbf{u}_{i,\text{nom}} = \left[S_{x,i}^{\text{des}} - S_{x,0}, S_{y,i}^{\text{des}} - S_{y,0} \right]^T$, the center of each stepping stone is designated as the desired step position.

The discrete MPC problem is formulated as follows:

$$\begin{aligned}
\underset{\tau_i, \mathbf{b}_i, \mathbf{u}_i}{\arg\min} \quad & \sum_{i=1}^{N} w_{\tau,i} \left\| \tau_i - \tau_{i,\text{nom}} \right\|^2 \\
& + \sum_{i=1}^{N} w_{b,i} \left\| \mathbf{b}_i - \mathbf{b}_{i,\text{nom}} \right\|^2 \\
& + \sum_{i=1}^{N} w_{u,i} \left\| \mathbf{u}_i - \mathbf{u}_{i,\text{nom}} \right\|^2 , \\
\text{s.t.} \quad & \tau_i \mathbf{b}_{i-1} - \mathbf{b}_i = \mathbf{u}_i - \mathbf{u}_{i-1} + \frac{\Delta \dot{\mathbf{v}}_{m,i}}{\omega} e^{\omega T_{i,\text{nom}}/2} ,
\end{aligned} \tag{29}$$

where $\Delta \dot{\mathbf{v}}_{m,i} = \left[\dot{x}_{m,i}^+ - \dot{x}_{m,i}^-, \dot{y}_{m,i}^+ - \dot{y}_{m,i}^- \right]^T$, $w_{\tau,i}$, $w_{b,i}$, $w_{u,i}$ are weight coefficients. In order to minimize the discrepancy between the actual step position and the desired step position, the weight $w_{u,i}$ is set to a relatively large value. Conversely, the step duration, being a more flexible parameter and primarily subject to adjustment, is associated with a smaller weight $w_{\tau,i}$. In addition, the subscript $(\cdot)_{\text{nom}}$ denotes the desired nominal value. We made an approximation in the constraint, where T_i in the last term on the right-hand side of the equation was replaced by $T_{i,\text{nom}}$.

To bridge the divergence between simplified model and the physical system, we implement a WBC strategy proposed in [18] as a low-level controller. This controller simultaneously tracks the desired centroidal trajectory and the foot-end trajectories generated by the MPC planner. The optimization problem is formulated as a quadratic programming(QP) problem with prioritized task execution. The WBC implemented

TABLE I
KUAVO SPECIFICATIONS

Mass	Normal height	W	Foot size
$44.9\,\text{kg}$	$0.78\,\text{m}$	$0.2\,\text{m}$	$0.2\,\text{m} \times 0.1\,\text{m}$

here extends the baseline WBC framework [18] through an arm regularization task. The task aims to drive the arm toward a desired joint angle by introducing a cost term:

$$w_{\text{arm}} \left\| \ddot{\boldsymbol{q}}_{\text{arm}} - \ddot{\boldsymbol{q}}_{\text{arm}}^{\text{des}} \right\|^2 \tag{30}$$

The desired acceleration is computed via a PD control law:

$$\ddot{\boldsymbol{q}}_{\text{arm}}^{\text{des}} = \boldsymbol{K}_p (\boldsymbol{q}_{\text{arm}}^{\text{des}} - \boldsymbol{q}_{\text{arm}}) + \boldsymbol{K}_d (\dot{\boldsymbol{q}}_{\text{arm}}^{\text{des}} - \dot{\boldsymbol{q}}_{\text{arm}}) \tag{31}$$

where $\boldsymbol{q}_{\text{arm}}$, $\dot{\boldsymbol{q}}_{\text{arm}}$, and $\ddot{\boldsymbol{q}}_{\text{arm}}$ denote the joint angle, joint velocity, and joint acceleration vector, respectively, and $(\cdot)^{\text{des}}$ describes the desired state. The controller assumes sufficient actuator torque capacity to execute generated motions, explicitly formulated through the omission of torque constraints in the QP formulation. This simplifying assumption facilitates controller synthesis while acknowledging potential implementation limitations through torque saturation effects in practical applications.

V. RESULTS

This section demonstrates the capability of the proposed hierarchical control framework in generating adaptive bipedal locomotion. The motion generation is achieved through simultaneous optimization of step duration and step position across stepping stones with elevation variations. When integrated with the WBC, the framework exhibits robust performance against terrain irregularities and external disturbances. Our tests were conducted in the physics-based simulation in MuJoCo [19] at 1KHz control frequency. Experimental validation was conducted on KUAVO (Version 4.0), a newly developed humanoid robot featuring upgraded actuation and sensing modules (Fig. 1). The detailed specifications related to this work is illustrated in Table I. Normal height here is the distance from the hip yaw joint to the ground when KUAVO is standing normally. The size of the stones in all tests is 0.2 m by 0.14 m.

We first established the baseline relative positions $\boldsymbol{p}^{\text{init}}$ between adjacent stepping stones. Subsequently, we introduced terrain disturbance $\boldsymbol{p}^{\text{dist}}$ in all three spatial directions, along with angular perturbations θ in the z-direction, to generate the actual stepping stones. Considering the spacing between the robot's left and right feet, the additional offset $W_{l/r}$ is added and $W_{l/r} = \pm W$. The detailed terrain information used in the experiments is summarized in Table II. Uniformly distributed random values are represented using $U[\cdot, \cdot]$.

We first validated the proposed framework across diverse terrains and operational conditions, followed by controlled

TABLE II
EXPERIMENT SCENARIOS

	$\boldsymbol{p}^{\text{init}}$ (cm)	θ (rad)	$\boldsymbol{p}^{\text{dist}}$ (cm)
a	[20, 0, 0]	0.0	periodic z=±17
b	[20, 0, 10]	0.2/-0.2	$U([-2.5,2.5]\times[-2.5,2.5]\times[-5,5))$
c	[20, 0, 0]	0	[0, 0, 0]
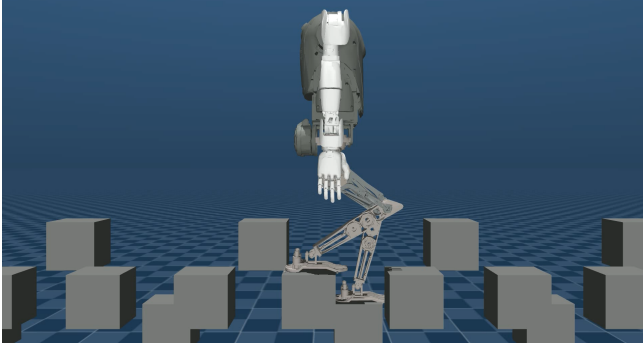
(a) KUAVO navigates a series of periodically arranged stepping stones, with neighboring stones spaced $\pm 17\,\text{cm}$ apart in the z direction.
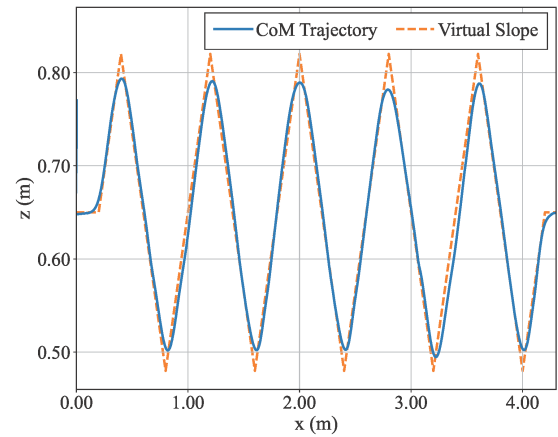
(b) The blue dashed line and orange dashed line indicate the CoM trajectory and piecewise virtual slopes projected in the xz plane.

Fig. 5. KUAVO traverses over the stepping stones with periodic elevation.

comparative studies to evaluate the theoretical formulations of the proposed model in Section II and III. To balance the planner's performance and solution computational, the prediction horizon was set to a full stride duration, such that the MPC's prediction encompassed both left and right stepping phases within a complete gait cycle. The optimization problem was formulated using the Drake library [20]. All tests are performed on a 12th Gen Intel i7 processor with 64GB of RAM. In this work, the average solver time is 0.9784 ms for MPC and 0.5881 ms for WBC, including the condition with terrain unevenness and force disturbances.

In the first validation, the proposed approach was employed in two different scenarios and then evaluate its robustness under unexpected force disturbances. Detailed experimental settings are shown in Table II.

Scenario a: To explicitly demonstrate the CoM trajectory generated by the proposed MPC-based optimization architecture, the KUAVO humanoid robot was programmed to traverse periodic stepping stones with a periodic vertical offset of 17 cm between adjacent stones (Fig. 5). As illustrated in Fig. 5(b), even when navigating uneven terrain with varying elevations, the CoM trajectory remains closely aligned with the direction of the constructed piecewise slopes. Notably, in the absence of PS-LIPM compensation or ALIP parameter adjustments, the robot failed to stabilize on this terrain and collapsed within 40th step, highlighting the critical role of the proposed method.

Scenario b: In this scenario, the terrain was constructed with stepping stones arranged in a non-periodic three-dimensional configuration by relatively random placement in all directions. Additionally, the challenge complexity was enhanced through varied orientations and height differentials among the stepping stones, as depicted in Fig. 6. The KUAVO successfully travel this uneven terrain while maintaining an exceptionally low average position error E_{avg} = 0.017 m. Fig. 7 comparatively shows three critical datasets: the actual step positions (S), theoretical target positions

corresponding to stepping stone centroids (S^{des}), and the corresponding trajectories of both the CoM and DCM.
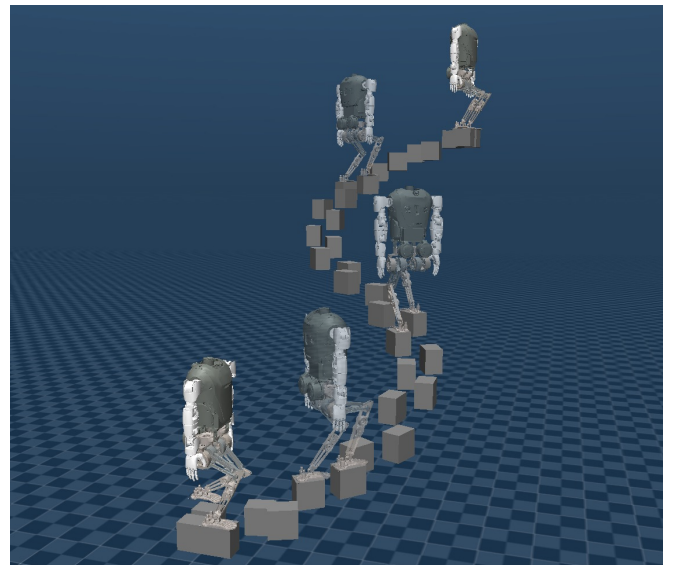

Fig. 6. KUAVO traverses over randomly arranged 3D stepping stones, where adjacent stones have a rotation angle of 0.2 radians around the z-axis. The maximum random displacement amplitudes in the 3D space are [0.05, 0.05, 0.10] m along the x, y, and z axes respectively.

Scenario c: This scenario validated the robustness of the hierarchical control framework by applying several external forces during walking. Unexpected external forces were applied in the sagittal plane: a backward force of 50 N at around 6 s and a forward force of 60 N at around 10 s. As shown in Fig. 9, by adjusting the duration of the steps, the controller gradually brought the DCM back to normal values.

In the second validation, three experimental trials were compared on the same terrain without any disturbance of the terrain, where $\boldsymbol{p}^{\text{init}} = [20, 0, 0]$. The robot successfully traversed over the terrain with $\alpha = 0$ and $\alpha = 0.5$, but it failed at 36th step with $\alpha = 1$.
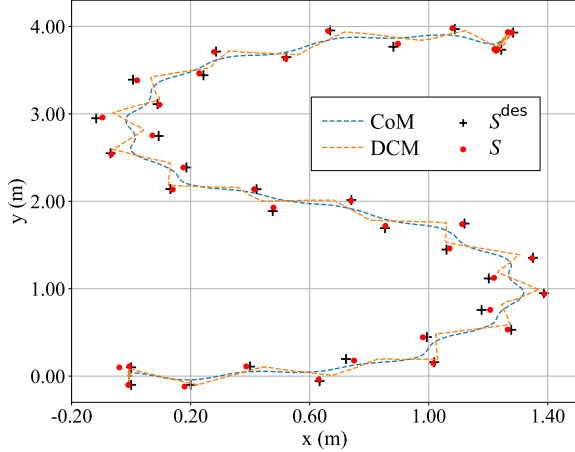
Fig. 7. Profiles of the actual step positions (red circles) and their corresponding desired targets (black crosses) as KUAVO traverses randomly arranged 3D stepping stones. The red dashed line represents the DCM trajectory, while the blue dashed line represents the CoM trajectory.

To quantify planning performance, we introduced the average step position deviation metric E_{avg}, representing the average deviation between the actual and desired step positions. The E_{avg} value observed at $\alpha = 0.5$ ($E_{avg} = 0.012$ m) is smaller than that at $\alpha = 0$ ($E_{avg} = 0.023$ m). Fig. 10 illustrates the DCM variation curves during the process, indicating that the DCM and the CoM control are optimal at $\alpha = 0.5$.

The third validation is to evaluate the superiority of PS-LIPM over conventional LIPM. We compared the average step position deviation E_{avg} for walking on elevation-disturbed stepping stones with and without PS-LIPM, where $\boldsymbol{p}^{\text{init}} = [20, 0, 0]$ cm, $\theta = 0$ and terrain disturbance in z
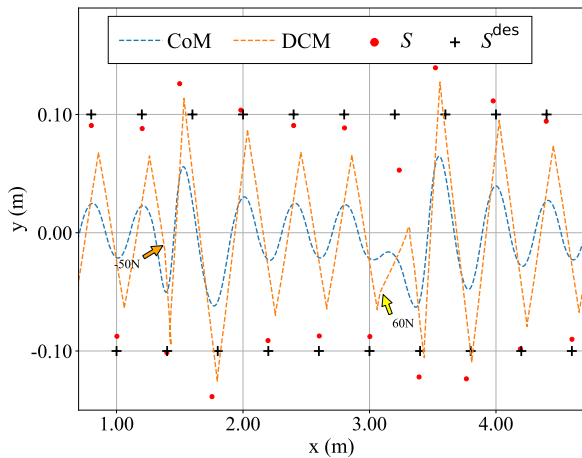

Fig. 8. The evolution of the DCM and CoM when encountering external disturbances. The actual step position will significantly deviate from the desired position when subjected to external perturbations, and it will return to the normal position after a period of adjustment.
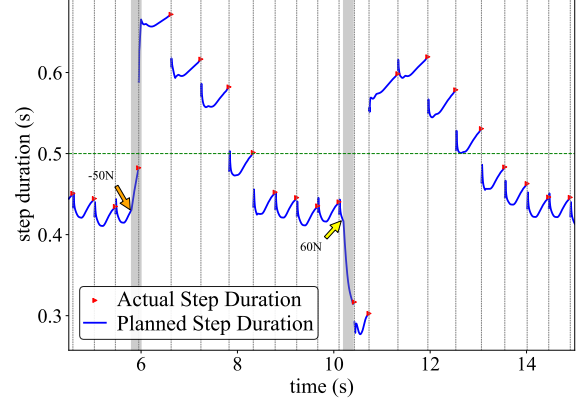

Fig. 9. The MPC planner optimizes the step duration to maintain the robot's stability. The gray shaded area indicates the duration of the external forces implied. The vertical gray lines mark the touch-down moments of walking steps.
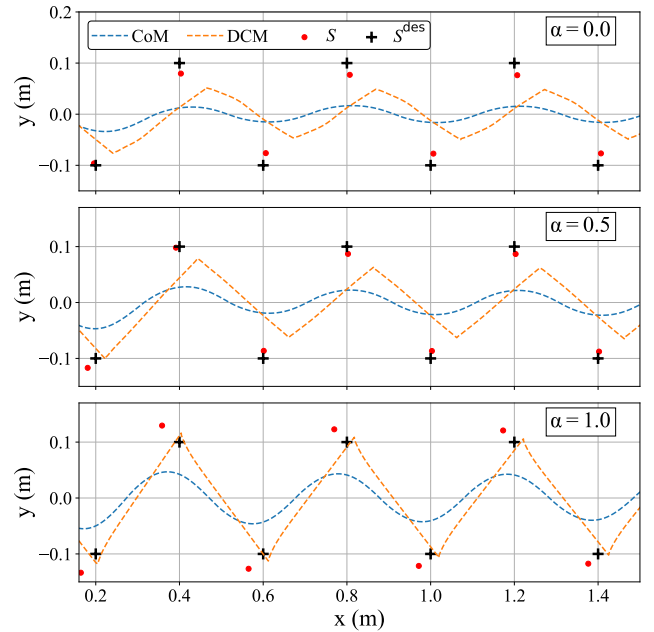

Fig. 10. Profiles of the DCM and CoM for G-ALIP coefficients of 0, 0.5, and 1. The actual step positions are closest to the desired positions when $\alpha = 0.5$.

direction is $U[-10, 10]$ (cm). The comparison of E_{avg} is depicted in Fig. 11. Data clusters without PS-LIPM (conventional LIPM, red-shaded area) exhibit systematically higher positional errors compared to PS-LIPM implementations (blue-shaded area) across equivalent elevation disturbances.

As elevation disturbances exceed 0.15 m, the deviation in the red-shaded area increases more sharply, indicating a more significant degradation in performance without PS-LIPM. In contrast, the blue-shaded area is narrower as terrain unevenness increases, suggesting that the robot's performance is more consistent with PS-LIPM. This improvement in accuracy and consistency highlights the effectiveness of PS-LIPM

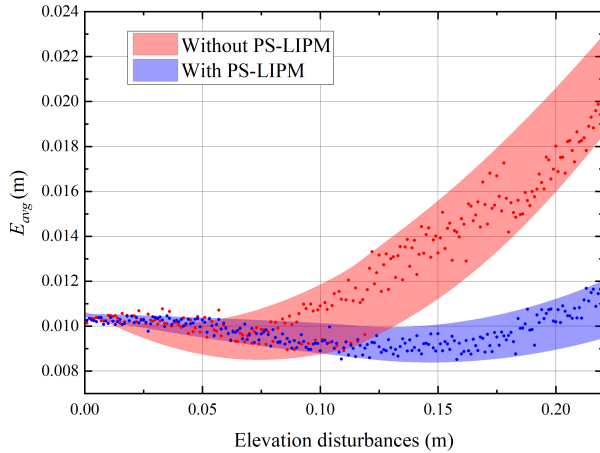in enhancing robotic mobility in challenging environments.

Fig. 11. The average step position deviation E_{avg} comparison profiles under terrain unevenness increases. The red-shaded area corresponds to conventional LIPM (without PS-LIPM) implementations, contrasting with PS-LIPM's performance profile in blue.

These investigations confirm that the modified MPC-based optimization architecture paradigm demonstrates enhanced adaptability to uneven terrain scenarios compared with conventional implementations.

VI. CONCLUSIONS

This work presents a hierarchical MPC-WBC framework for robust bipedal locomotion on uneven terrains, advancing theoretical and practical capabilities through two key innovations. First, the proposed PS-LIPM overcomes conventional LIPM limitations by dynamically adjusting the CoM height during single-step cycles to accommodate terrain elevation variations. Second, the G-ALIP model generalizes centroidal momentum regulation, enabling CoM velocity compensation through CAM adjustments. The derived DCM step-to-step dynamics explicitly characterizes step transitions and enables simultaneous optimization of step positions and durations in MPC. Experimental evaluations demonstrate the adaptability of three-dimensional rotational stepping stones under random positional disturbances (maximum amplitude: [0.05, 0.05, 0.10] m) and robustness against external disturbances up to 60 N. Comparative studies further confirm that PS-LIPM and G-ALIP outperform baseline methods, as evidenced by a lower average step position deviation.

REFERENCES

[1] M. Khadiv, A. Herzog, S. A. A. Moosavian, and L. Righetti, "Walking control based on step timing adaptation," *IEEE Transactions on Robotics*, vol. 36, no. 3, pp. 629–643, 2020.

[2] S. Kajita, F. Kanehiro, K. Kaneko, K. Yokoi, and H. Hirukawa, "The 3d linear inverted pendulum mode: A simple modeling for a biped walking pattern generation," in *Proceedings 2001 IEEE/RSJ International Conference on Intelligent Robots and Systems. Expanding the Societal Role of Robotics in the the Next Millennium (Cat. No. 01CH37180)*, vol. 1. IEEE, 2001, pp. 239–246.

[3] A. Massah, A. Sharifi, Y. Salehinia, and F. Najafi, "An open loop walking on different slopes for nao humanoid robot," *Procedia Engineering*, vol. 41, pp. 296–304, 2012.

[4] Y. Shi, P. Wang, M. Li, X. Wang, Z. Jiang, and Z. Li, "Model predictive control for motion planning of quadrupedal locomotion," in *2019 IEEE 4th international conference on advanced robotics and mechatronics (ICARM)*. IEEE, 2019, pp. 87–92.

[5] G. Romualdi, S. Dafarra, G. L'Erario, I. Sorrentino, S. Traversaro, and D. Pucci, "Online non-linear centroidal mpc for humanoid robot locomotion with step adjustment," in *2022 International Conference on Robotics and Automation (ICRA)*. IEEE, 2022, pp. 10 412–10 419.

[6] J. Englsberger, C. Ott, and A. Albu-Schäffer, "Three-dimensional bipedal walking control using divergent component of motion," in *2013 IEEE/RSJ International Conference on Intelligent Robots and Systems*. IEEE, 2013, pp. 2600–2607.

[7] M. Khadiv, S. Kleff, A. Herzog, S. A. A. Moosavian, S. Schaal, and L. Righetti, "Stepping stabilization using a combination of dcm tracking and step adjustment," in *2016 4th International Conference on Robotics and Mechatronics (ICROM)*. IEEE, 2016, pp. 130–135.

[8] T. Kamioka, H. Kaneko, T. Takenaka, and T. Yoshiike, "Simultaneous optimization of zmp and footsteps based on the analytical solution of divergent component of motion," in *2018 IEEE international conference on robotics and automation (ICRA)*. IEEE, 2018, pp. 1763–1770.

[9] J. A. Castano, Z. Li, C. Zhou, N. Tsagarakis, and D. Caldwell, "Dynamic and reactive walking for humanoid robots based on foot placement control," *International Journal of Humanoid Robotics*, vol. 13, no. 02, p. 1550041, 2016.

[10] P. Kryczka, P. Kormushev, N. G. Tsagarakis, and D. G. Caldwell, "Online regeneration of bipedal walking gait pattern optimizing footstep placement and timing," in *2015 IEEE/RSJ International Conference on Intelligent Robots and Systems (IROS)*. IEEE, 2015, pp. 3352–3357.

[11] Z. Xiang, V. Paredes, G. A. Castillo, and A. Hereid, "Adaptive step duration for precise foot placement: Achieving robust bipedal locomotion on terrains with restricted footholds," *arXiv preprint arXiv:2403.17136*, 2024.

[12] N. Bohórquez and P.-B. Wieber, "Adaptive step duration in biped walking: a robust approach to nonlinear constraints," in *2017 IEEE-RAS 17th International Conference on Humanoid Robotics (Humanoids)*. IEEE, 2017, pp. 724–729.

[13] Y. Shi, X. He, W. Zou, B. Yu, L. Yuan, M. Li, G. Pan, and K. Ba, "Multi-objective optimal torque control with simultaneous motion and force tracking for hydraulic quadruped robots," *Machines*, vol. 10, no. 3, p. 170, 2022.

[14] H. Chai, Y. Li, R. Song, G. Zhang, Q. Zhang, S. Liu, J. Hou, Y. Xin, M. Yuan, G. Zhang, *et al.*, "A survey of the development of quadruped robots: Joint configuration, dynamic locomotion control method and mobile manipulation approach," *Biomimetic Intelligence and Robotics*, vol. 2, no. 1, p. 100029, 2022.

[15] M. Dai, X. Xiong, and A. Ames, "Bipedal walking on constrained footholds: Momentum regulation via vertical com control," in *2022 International Conference on Robotics and Automation (ICRA)*, 2022, pp. 10 435–10 441.

[16] G. Gibson, O. Dosunmu-Ogunbi, Y. Gong, and J. Grizzle, "Terrain-adaptive, alip-based bipedal locomotion controller via model predictive control and virtual constraints," in *2022 IEEE/RSJ International Conference on Intelligent Robots and Systems (IROS)*, 2022, pp. 6724–6731.

[17] O. Dosunmu-Ogunbi, A. Shrivastava, G. Gibson, and J. W. Grizzle, "Stair climbing using the angular momentum linear inverted pendulum model and model predictive control," in *2023 IEEE/RSJ International Conference on Intelligent Robots and Systems (IROS)*, 2023, pp. 8558–8565.

[18] J. Shen, J. Zhang, Y. Liu, and D. Hong, "Implementation of a robust dynamic walking controller on a miniature bipedal robot with proprioceptive actuation," in *2022 IEEE-RAS 21st International Conference on Humanoid Robots (Humanoids)*. IEEE, 2022, pp. 39–46.

[19] E. Todorov, T. Erez, and Y. Tassa, "Mujoco: A physics engine for model-based control," in *2012 IEEE/RSJ International Conference on Intelligent Robots and Systems*. IEEE, 2012, pp. 5026–5033.

[20] R. Tedrake and the Drake Development Team, "Drake: Model-based design and verification for robotics," 2019. [Online]. Available: https://drake.mit.edu